NANO LETTERS

Letter

pubs.acs.org/NanoLett

Nerve Cells Decide to Orient inside an Injectable Hydrogel with Minimal Structural Guidance

Jonas C. Rose,[†] María Cámara-Torres,[†] Khosrow Rahimi,[†] Jens Köhler,[†] Martin Möller,[†,‡] and Laura De Laporte*[,†]

[†]DWI – Leibniz-Institute for Interactive Materials, 52074 Aachen, Germany

[‡]Institute for Technical and Macromolecular Chemistry, RWTH, 52062 Aachen, Germany

Supporting Information

ABSTRACT: Injectable biomaterials provide the advantage of a minimally invasive application but mostly lack the required structural complexity to regenerate aligned tissues. Here, we report a new class of tissue regenerative materials that can be injected and form an anisotropic matrix with controlled dimensions using rod-shaped, magnetoceptive microgel objects. Microgels are doped with small quantities of superparamagnetic iron oxide nanoparticles (0.0046 vol %), allowing alignment by external magnetic fields in the millitesla order. The microgels are dispersed in a biocompatible gel precursor and after injection and orientation are fixed inside the matrix hydrogel. Regardless of the low volume concentration of the microgels below 3%, at which the geometrical constrain for orientation is still minimum, the generated macroscopic unidirectional orientation is strongly sensed by the cells resulting in parallel nerve extension. This finding opens a new, minimal invasive route for therapy after spinal cord injury.

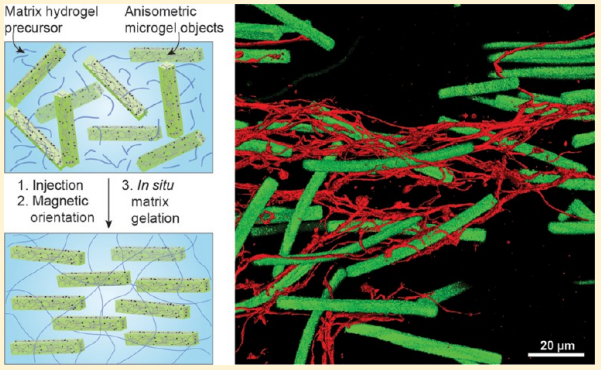

KEYWORDS: *Nerve growth, tissue regeneration, injectable hydrogel, anisotropy, magnetic alignment, microgels, magnetic nanoparticles*

In vivo, cells are surrounded by an extracellular matrix (ECM) that provides biological, mechanical, and structural support. The ECM functions as a spatiodynamic bioscaffold, which is created and maintained by the surrounding cells and in return influences the cellular signaling, architecture, and functionality.[1] In the case of irreversible tissue damage, an artificial matrix can be applied for healing. This matrix needs to address and mimic the conditions of the respective cell niche(s) in order to induce and support the regenerative capacity of endogenous surrounding and invading cells, or cell transplants.[2] Therefore, micron-scale and modular approaches are developed to fabricate complex functional biomaterial structures.[3] Moreover, multiple implantable constructs with aligned channels[4] or fibers[5] have been designed and applied to provide cell guidance, for example, for the purpose of spinal cord injury. However, depending on the type of damaged tissue, the severity of the disorder, and the time after injury, the application of either a preformed implant or an injectable liquid that forms a matrix in situ is desired. Injectable matrices are minimally invasive and are especially suitable to support healing of acute trauma-induced injuries of sensitive tissues, such as spinal cord,[6] myocardium,[7] and brain,[8] as remaining functional tissue should not be further impaired.[9] The advantage of injectable materials is that they can adopt any desired shape for the regeneration of various tissues, including bone,[10] cartilage,[11] and wound healing.[12]

As tissues comprise a complex, anisotropic, and hierarchical structure, regenerative matrices have to provide the correct architecture to guide cell organization during the healing process.[2b,13] In the case of peripheral and spinal nervous tissue, linear structures need to be designed. This can be achieved by aligning diamagnetic ECM–protein hydrogels, such as collagen or fibrin, in high magnetic fields (>4.5 T).[14] In vivo, Tranquillo et al. demonstrated more regenerating nerve cells in the peripheral nervous system when filling the hollow collagen tubes from Integra Life Sciences with a collagen gel that was aligned in a magnetic field of 9.4 T.[15] In contrast, most current injectable materials lack the ability to template complex tissue structures with directionally organized functions and mechanical properties. To our knowledge, only a few examples have been proposed for injectable materials that provide directional control. On the one hand, peptide hydrogels with monodomain regions of oriented fiber bundles, as introduced by Zhang et al.,[16] demonstrated aligned neurite outgrowth of dorsal root ganglions (DRGs) in vitro.[17] On the other hand, composite hydrogels have been described with polydisperse magnetically aligned chains of spherical iron oxide particles in Matrigel, supplying structure for orientation of single fibroblasts and PC12 neuron-like cells, both parallel and perpendicular to the

Received: March 16, 2017
Published: March 22, 2017

DOI: 10.1021/acs.nanolett.7b01123
Nano Lett. 2017, 17, 3782–3791

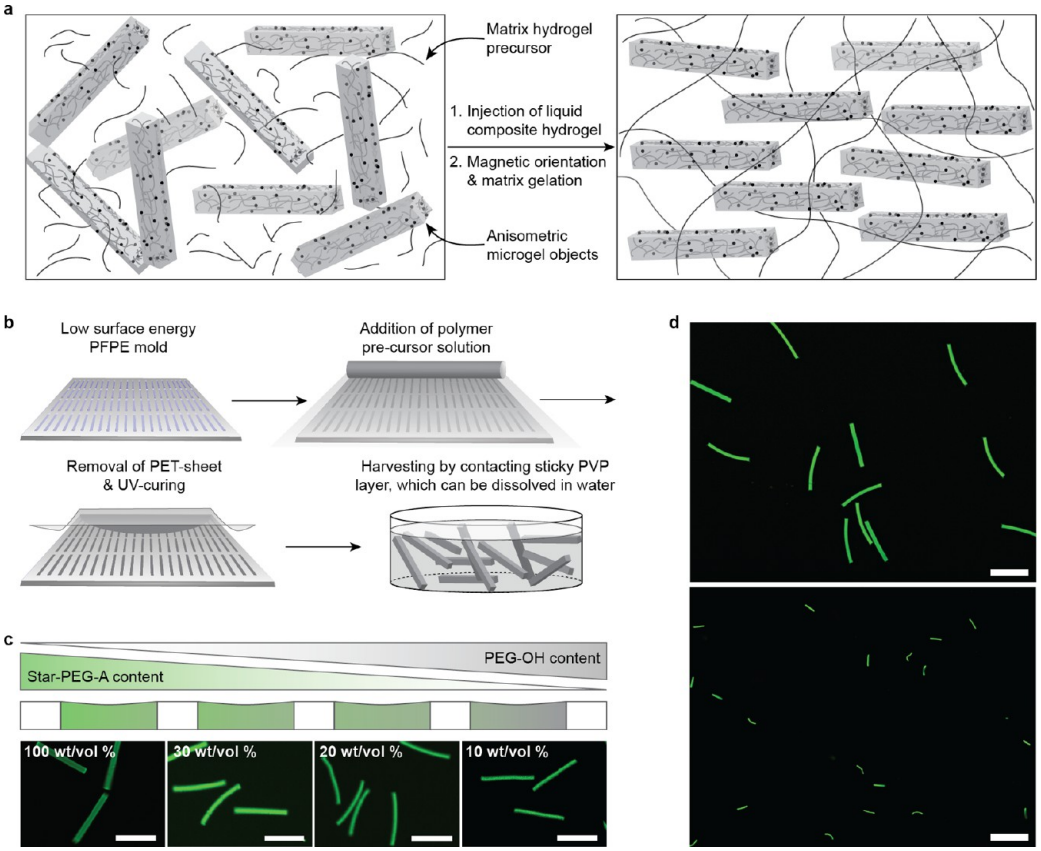

Figure 1. Preparation of soft, anisometric microgels. (a) Our approach of an injectable hybrid hydrogel (Anisogel), which generates a unidirectional structure in situ by aligning rod-shaped, magnetoceptive, soft microgels within an even softer surrounding hydrogel matrix. After injection, the liquid surrounding hydrogel precursor solution is cross-linked to fix the microgel orientation, representing barriers, which can linearly direct cell ingrowth. (b) Soft microgels were prepared by a mold-based soft lithography technique, involving a repelling PFPE mold, upon which a polymer precursor solution was cast and captured within the cavities. After UV-curing, microgels were retrieved by a sticky water-soluble PVP layer. Soft, heterogeneous, highly water-swollen anisometric microgels were fabricated with various star-PEG-A concentrations (c) and dimensions (d): top 5 × 5 × 50 μm^3, bottom 1 × 1 × 10 μm^3). All scale bars are 50 μm. Green color: fluorescein.

direction of the particle strings.[18] The alignment of these magnetic particles was proposed to induce orientation of collagen fibers within a collagen hydrogel for guiding cells.[19] As concentrations of magnetic iron oxide particles in the order of 1.5 mM iron decrease viability of sensitive cells and reduce the ability to form neurites,[20] it is essential to reduce the amount of iron oxide, incorporated into these regenerative systems.

Here, we demonstrate a new type of anisotropic and injectable hybrid hydrogel, called an Anisogel. An Anisogel is a biocompatible and soft dual hydrogel system containing (i) microgels that are monodisperse, magneto-receptive, rod-shaped, and soft and (ii) a surrounding hydrogel matrix, which cross-links in situ and fixes the oriented microgels (Figure 1a). Small amounts of superparamagnetic iron oxide nanoparticles (SPIONs) are incorporated inside the microgels to order them unidirectionally in the presence of a low external magnetic field in the millitesla range. We design microgels with specific dimensions to induce an ultrahigh magnetic response (UHMR[21]), which allows a significant reduction of SPIONs, circumventing iron-cytotoxicity. Furthermore, the microgels can be tailored in regard to their mechano-physical properties by modifying the prepolymer composition. Following the alignment, the oriented microgels are interlocked within a cross-linking hydrogel, creating an Anisogel. The soft magneto-responsive microgels function as nonadherent cell barriers in an even softer surrounding cell-adhesive fibrin matrix. Thereby, the Anisogel approach is hierarchically designed bottom-up with building blocks in the nano- to micro- to macroscale. With this material, we investigate how sensitive fibroblasts and nerve cells are to structural guidance cues in 3D and what the minimal amount of required signals is to prompt their decision to grow in an aligned manner.

Fabrication of Anisometric Microgels with Controlled Mechano-Physical Properties. The rod-shaped microgels were produced with a mold-based soft lithography approach (Figure 1b[22]), applying six-armed star-shaped poly(ethylene oxide-*stat*-propylene oxide) with acrylate end groups (star-PEG-A) as the reactive prepolymer. Star-PEG has previously demonstrated to reduce the formation of fibrous capsules and no inflammatory responses were detected in vivo.[23] The liquid star-PEG-A prepolymer was cast into a highly repelling perfluoropolyether (PFPE) mold[24] in the presence of a photoinitiator and fluorescein *o*-acrylate. UV-curing of the solution-filled features resulted in fluorescent microgels with precise mold replication (Supporting Information Figure 1a). The individual microgel objects were removed from the mold by putting them in contact with a sticky polyvinylpyrrolidone layer that can be dissolved in water afterward. Although several techniques have been developed to fabricate anisometric micron-scale solid particles over the past decade,[22,25] it is still challenging to produce anisometric, highly water-swollen, soft microgels. In the case of water or DMSO as a diluent for the

DOI: 10.1021/acs.nanolett.7b01123
Nano Lett. 2017, 17, 3782−3791

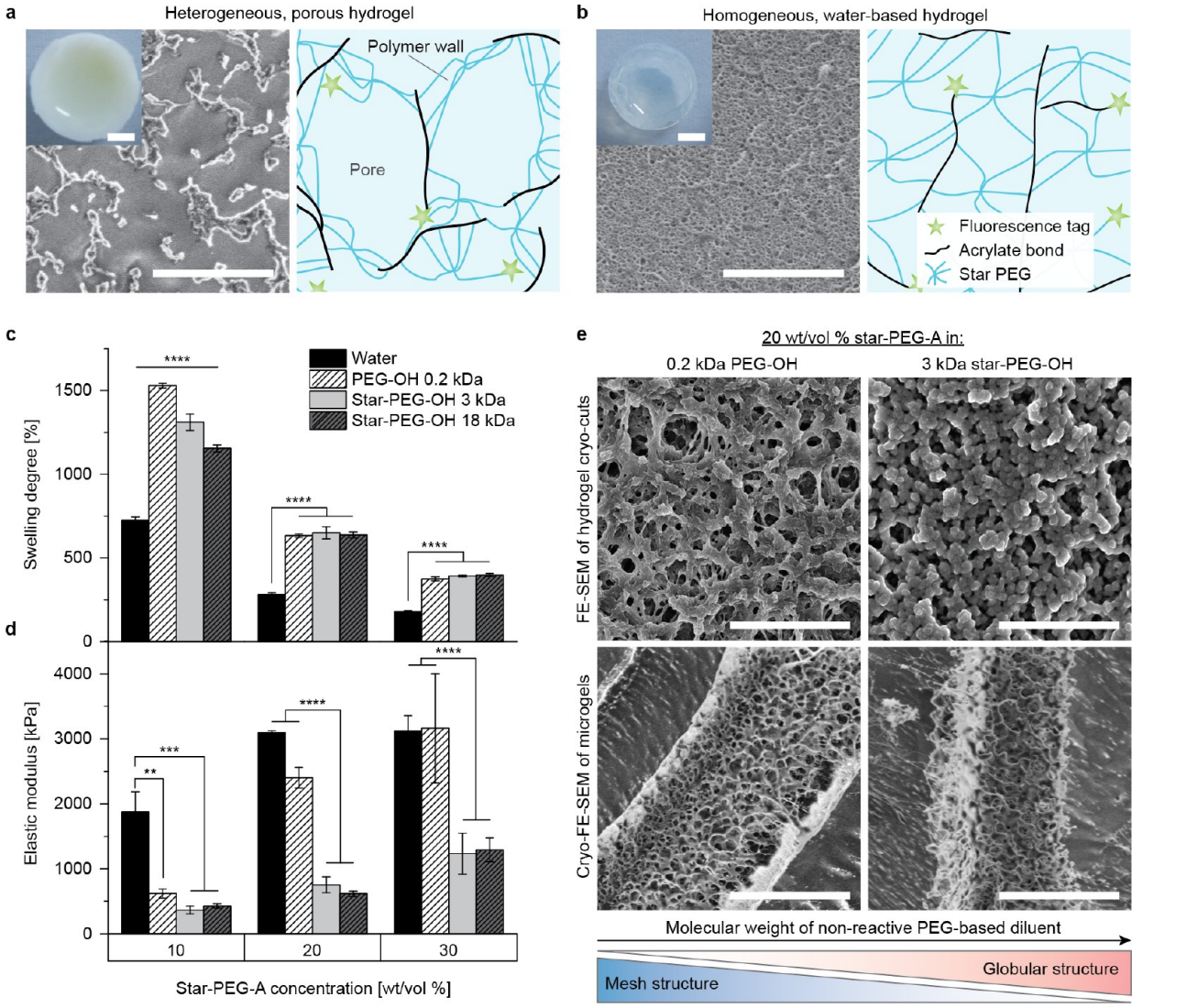

Figure 2. Characterization of hydrogels. (a) Dilution of star-PEG-A (20 wt/vol %) with a nonreactive PEG-based diluent (here 0.2 kDa PEG-OH) led to a visually white, heterogeneous hydrogel, consisting of water-filled micron-scale voids and nanoporous polymer regions, whereas by diluting with water (b) a homogeneous hydrogel was formed with a transparent appearance and pores in the nanometer-scale. Elastic modulus (c) and swelling degree (d) of water-diluted hydrogels in comparison to polymer-diluted hydrogels. (e) FE-SEM analysis of cryo-cuts of hydrogels showed a difference in the gel morphology, depending on the type of diluent. The voids of polymer-diluted hydrogels were also found in fabricated microgels. Data presented as average ± s.d. and statistical significance performed using two-way ANOVA with Bonferroni comparison (**$p < 0.01$; ***$p < 0.001$; ****$p < 0.0001$). Scale bars in macroscopic hydrogels in (a) and (b) are 2 mm and 5 μm in FE-SEM images (a,b,e).

star-PEG-A precursor, evaporation and an increase in surface tension caused incomplete filling of the mold cavities (Supporting Information Table 1, Supporting Information Figure 1b). Previously, this problem has been reduced by decreasing the temperature while molding, forming soft homogeneous microgels.[26] We opted to blend the reactive star-PEG-A with a second nonvolatile, nonreactive polymer-diluent that was washed out after cross-linking. This enabled us to generate soft microgels with low polymer contents down to 10 wt/vol % (Figure 1c), which provided us an adequate range of polymer densities for in vivo applications.[27] Typical sizes of the microgel objects, used in this report, were 50 × 5 × 5 μm^3 and 10 × 1 × 1 μm^3 (Figure 1d).

Cross-linking of the star-PEG-A in a polymer blend resulted in reaction-induced phase decomposition (RIPD, Figure 2a[28]). Mechanistically, the two polymers phase separated during cross-linking of the reacting phase to maintain the minimal Gibb's free energy (ΔG) according to the Flory–Huggins theory for polymer blends. This well-known phenomenon enabled us to control the mechano-physical properties of the microgels and thus the interaction with cells.[2a,29] Three different nonreactive polymers were used in liquid form as a diluent and resulted in precise molding: linear poly(ethylene glycol) (PEG-OH) with low MW (0.2 kDa) or six-armed star-shaped poly(ethylene oxide-*stat*-propylene oxide) (star-PEG-OH) with higher MWs (3 and 18 kDa). To facilitate characterization of their structural and mechanical properties, macroscopic hydrogel disks (12 mm × 1 mm) were prepared. In all cases, the inert diluent was completely extracted after curing of the hydrogel by incubation with water (3 times 30 min), indicating fast mass transport of even large molecules, such as 18 kDa star-PEG-OH (Supporting Information Figure 2). Hydrogels fabricated with water as diluent were transparent (Figure 2b), whereas hydrogels made with the polymer blend

DOI: 10.1021/acs.nanolett.7b01123
Nano Lett. 2017, 17, 3782–3791

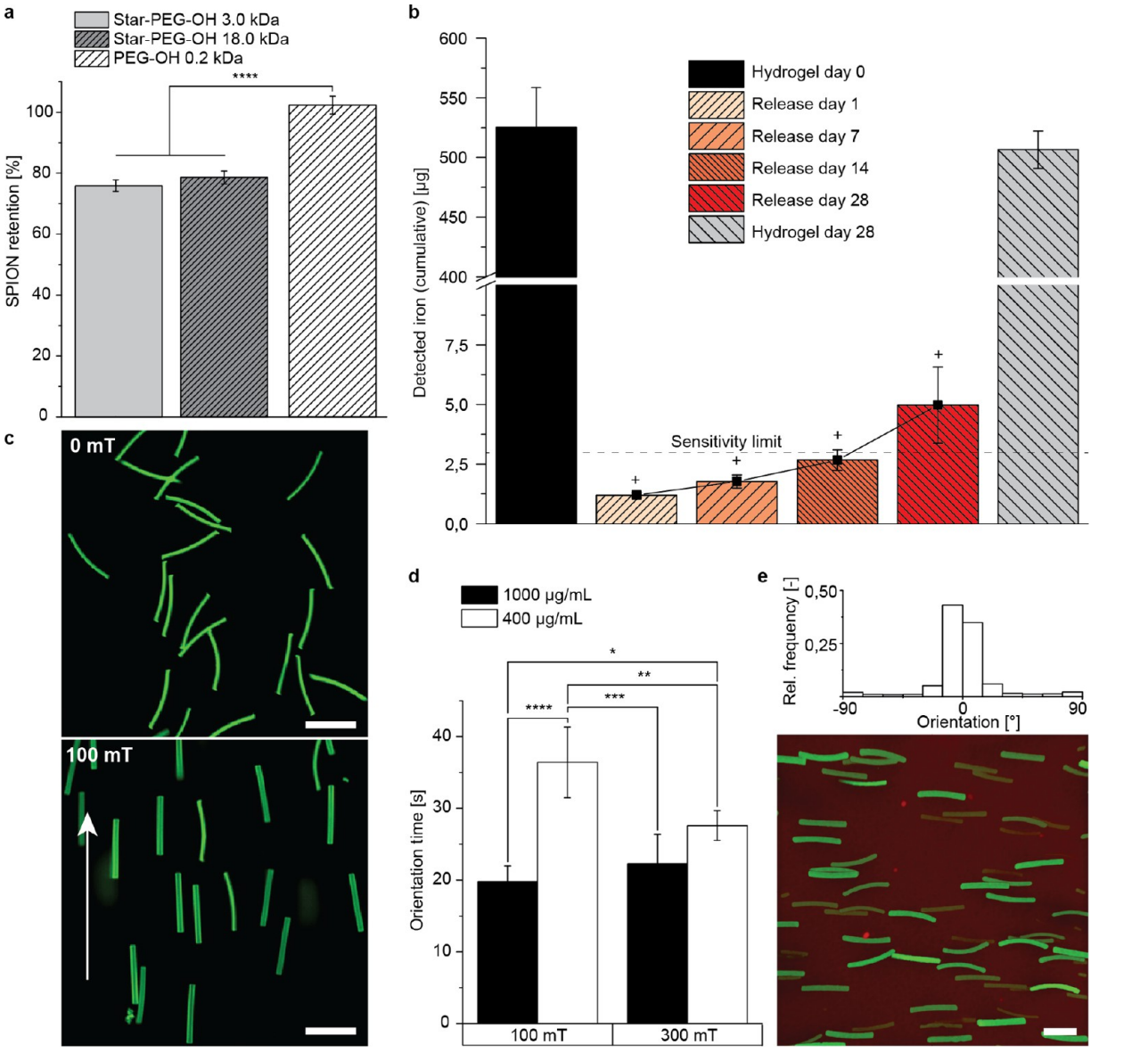

Figure 3. Characterization of magnetoceptive microgels. (a) SPION-retention of 20 wt/vol % star-PEG-A hydrogels, blended with different polymer diluents, revealed a very high retention capacity, especially for PEG-OH 0.2 kDa based gels. (b) Released iron amount over time (cumulative) from hydrogels, consisting of 20 wt/vol % star-PEG-A diluted with PEG-OH 0.2 kDa, including the iron amounts after extraction and after incubation for 28 days (+ means below sensitive region of device). (c) Incorporation of 400 μg/mL randomly distributed SPIONs allowed for alignment in a 100 mT magnetic field. (d) When the microgel direction along the magnetic field lines remained coherent (<0.1%/s coherency change over 5 s), they were considered to be aligned, which allowed the determination of orientation times (Figure S10). (e) Fixation of magnetically aligned microgels in a surrounding fibrin gel and the distribution histogram by OrientationJ (Fourier gradient). Scale bars are 50 μm. Green, fluorescein; red, Rhodamine-labeled fibrinogen. Data presented as average ± s.d. and statistical significance performed using two-way ANOVA with Bonferroni comparison (*p < 0.05; **p < 0.01; ***p < 0.001; ****p < 0.0001).

demonstrated a completely white appearance before and after extraction, indicating significant structural heterogeneity (Figure 2a, Supporting Information Figure 3). As incubation of dried heterogeneous hydrogels in the inert polymer-diluent did not result in swelling, we confirmed the incompatibility of the cross-linked network chains with the diluent after gelation (Supporting Information Figure 4). Visualizing the microscopic cross sections by cryo-electron micrographs revealed a structure with pores up to the micrometer scale. The microporosity was reduced at higher star-PEG-A content and increased when PEG-OH 0.2 kDa was employed (Supporting Information Figure 5). It can be concluded that cross-linking of applied polymer blends resulted in a double network, whose domains of the cross-linked star-PEG-A network form a mesoscopic framework with pores in the microrange, which can facilitate diffusion of nutrients and cell signaling molecules.[28,30]

The heterogeneous hydrogels contained an elastic modulus in the kPa range and a high degree of swelling in water. The elastic modulus was lower compared to the water-diluted hydrogels despite containing the same amount of cross-linked polymer (Figure 2c). One exception was 30 wt/vol % star-PEG-A, blended with PEG-OH 0.2 kDa, which had a similar modulus as the water-diluted variant. When comparing the different blend hydrogels, we observed that the hydrogels, prepared with low MW PEG-OH, were significantly stiffer compared to the hydrogels, fabricated with the higher MW star-

DOI: 10.1021/acs.nanolett.7b01123
Nano Lett. 2017, 17, 3782−3791

PEG-OH. This difference in stiffness was more distinct for higher star-PEG-A concentrations (20 and 30 wt/vol %), whereas there was no significant difference in swelling among the inert polymers at these concentrations (Figure 2d). For lower star-PEG-A (10 wt/vol %), no significant differences in stiffness were found between the nonreactive polymer diluents, but the degree of swelling increased with reduced MW of the diluent. These findings are in contrast with conventional water-based hydrogels, for which an increasing elastic modulus is associated with less water uptake.[31] This may be explained by differences in the hydrogel structures, as electron micrographs display two types of morphologies (Figure 2e, Supporting Information Figures 6 and 7). Dilution of star-PEG-A with both star-PEG-OHs (3 and 18 kDa) led to a coarser granular structure with smaller globules, whereas dilution with 0.2 kDa PEG-OH revealed a microscopic interconnected mesh structure, which was intensified with increasing star-PEG-A content. The mesh-like structure observed in the case of low MW PEG-OH may cause the enhanced stiffness's of the hydrogels, compared to blending with higher MW star-PEG-OH. The higher degree of swelling for decreasing MW of the inert polymer in the case of 10 wt/vol % star-PEG-A may be correlated to the presence of larger macroscopic pores (Supporting Information Figure 5). These structural differences might be due to the type of RIPD occurring. A spinodal decomposition network is known to be more regularly interconnected, whereas a binodal decomposition network characteristically consists of associated gel nuclei, giving it a more irregular globular structure.[32] Cryo-electron micrographs of microgels, composed of 20 wt/vol % star-PEG-A and different inert diluents verified that the microgels contained a similar heterogeneous appearance as the hydrogel disks, which enables us to control their properties for regenerative purposes (Figure 2e, Supporting Information Figure 8).

Alignment of Microgels by an External Magnetic Field. Alignment of the microgels was achieved by rendering them magnetic. Anionic-coated SPIONs (EMG700 by Ferrotec with 45.64% iron oxide in particles, determined by elemental analysis) were randomly dispersed in the prepolymer solution before molding and curing. Without an external magnetic field, the lack of unidirectional spin alignment of the SPIONs impedes a macroscopic magnetization of the microgels. Within a magnetic field, the magnetization becomes polarized and long-range dipolar interactions between the dispersed SPIONs cause a preferred orientation along the easy axis of the rodlike microgels. This induces microgel alignment parallel to the magnetic field.[21,33] The incorporation efficiency and retention of SPIONs were determined by elemental analysis of iron in macroscopic hydrogel disks after diluent extraction and after incubation in buffer (phosphate buffered saline (1X PBS)) for 4 weeks at 37 °C. SPIONs within a 20 wt/vol % star-PEG-A hydrogel network, fabricated by blending PEG-OH 0.2 kDa, were fully retained, despite complete removal of the PEG-diluent (Figure 3a, Supporting Information Figure 2). In comparison, hydrogels, prepared with 20 wt/vol % star-PEG-A, diluted with star-PEG-OH, lost more than 20 wt/vol % of the premixed SPIONs during extraction. This observation suggests that the SPIONs were better entrapped within the cross-linked hydrogel network when low MW PEG-OH was applied as nonreactive diluent compared to star-PEG-OH.[28] After extraction, we found that there was no significant release of SPIONs over a period of 4 weeks, which indicates a high SPION retention capacity of the heterogeneous hydrogel network (Figure 3b). Transmission electron microscopy (TEM) revealed that homogenization via ultrasonication yielded well-dispersed SPIONs with only a few aggregates throughout the microgel (1 μm diameter and 10 μm length, Supporting Information Figure 9).

The analysis of the magnetic response was performed with microgels fabricated with 20 wt/vol % star-PEG-A and 0.2 kDa PEG-OH as the diluent to obtain maximal SPION retention. The orientation time was determined via a software-based orientation analysis (ImageJ plugin OrientationJ), which evaluated every pixel of the image based on a structure tensor (Supporting Information Figure S10a). Distributing 400 μg SPIONs/mL, corresponding to 0.0046 vol %, randomly throughout the microgels (50 × 5 × 5 μm^3) resulted in longitudinal alignment in a magnetic field of 100 mT within 36.4 ± 4.9 s (Figure 3c,d, Supporting Information Figure 10b, Movie 1). Increasing the SPION concentration to 1000 μg/mL (0.0114 vol %) or increasing the magnetic field to 300 mT resulted in shorter orientation times of 19.8 ± 2.2 and 27.6 ± 2.1 s, respectively. Microgels with a concentration of 1000 μg/mL in 300 mT started to move within the dispersion and interact with each other, causing aggregation (Supporting Information Figure 10c, Movie 2). These observations are in contrast to a report by Nunes et al.,[34] which demonstrated that, prior to curing, magnetic prealignment of the SPIONs into chainlike structures was required to orient rod-shaped particles (aspect ratio below 3). As the magnetic response is mostly geometry-driven, the higher aspect ratio of the presented microgels (aspect ratio of 10) may explain the difference in observation. Previously, solid SPION-coated microrods with the same aspect ratio of 10 were demonstrated to exhibit an ultrahigh magnetic response (UHMR).[21] The measured orientation times here suggest that the dipole interactions between the SPIONs, distributed randomly inside the dimension-tailored microgels, were robust enough to obviate the need to prealign the SPIONs.[33b]

To interlock the oriented microgels, a surrounding hydrogel precursor solution was cross-linked. Both the kinetics of the magnetic response of the microgels and the gelation time of the matrix hydrogel were tuned to achieve optimal alignment. We chose human fibrin as a model for the surrounding cell-adhesive hydrogel and its gelation time was controlled to approximately 1 min by using a thrombin concentration of 0.125 U/mL to activate the fibrin precursor fibrinogen.[35] Oriented microgels were fixed inside a fibrin matrix (Figure 3e), creating a hybrid hydrogel with global unidirectional anisotropy (Anisogel).

Directed Cell and Nerve Growth in Injectable Anisotropic Hydrogel. The obtained Anisogel was then applied to induce directed cell growth. To influence the orientation of cell growth, microgels functioned as barriers that initially do not support cell ingrowth, which is in contrast to the surrounding hydrogel. Yet, microgels need to enable sufficient mass transport and degradation over time. Therefore, microgels with a star-PEG-A content of 20 wt/vol %, prepared with PEG-OH 0.2 kDa as diluent, were chosen for subsequent experiments, as these also demonstrated maximal SPION retention. To minimize cytotoxic effects, a low SPION concentration of 400 μg/mL was applied. The cytotoxicity of SPION-doped star-PEG-A hydrogels was tested in vitro by a cell viability assay (Supporting Information Figure 11a), revealing no release of cytotoxic hydrogel components over the course of 24 h. The hydrogel media extract did not reduce cell survival or proliferation rates over a period of 5 days. To

DOI: 10.1021/acs.nanolett.7b01123
Nano Lett. 2017, 17, 3782−3791

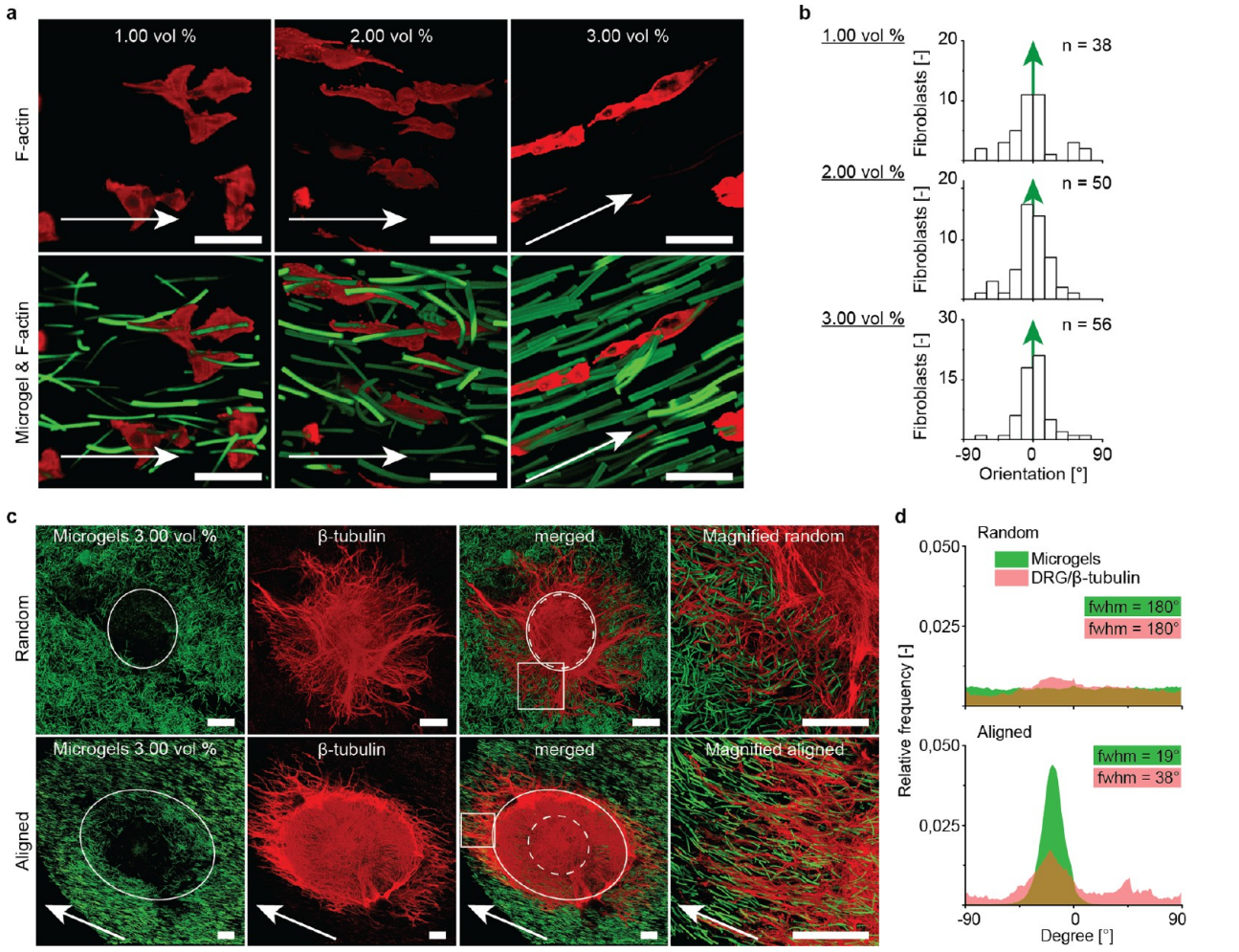

Figure 4. Ability of the Anisogel to align fibroblasts and guide nerves. Fibrin hydrogels were mixed with different concentrations (1.0, 2.0, and 3.0 vol %) of soft microgels, which aligned in a magnetic field of 130 mT. (a) Premixed fibroblasts extended along the longitudinal microgel axis (green, fluorescein), visible by the stretched F-actin filaments (red, Alexa Fluor 594 phalloidin), depending on the microgel concentration. (b) Quantification of single fibroblast orientation in the Anisogel with different microgel concentrations in relation to microgel orientation (green arrow), *n* meaning the total number of randomly analyzed cells from different gels. (c) DRGs were positioned in hydrogels with 3 vol % microgels (green, fluorescein), containing random or magnetically aligned microgels. *β*-tubulin staining (red, Alexa Fluor 633) revealed neurite outgrowth parallel to the aligned microgels (outside full white circle). (d) Distribution of neurite and microgel orientation, as well as the respective full width at half-maximum (fwhm). The white full circles mark from which distance neurite extension was quantified. The white dotted circle represents the edge of the DRG body. The white box marks the magnified regions, depicted on the right. Scale bars in (a) are 50 μm and in (c) are 200 μm.

study the effect of aligned microgels on cell morphology, L929 mouse-derived fibroblasts (500 cells/μL) were mixed within the Anisogel solution before cross-linking and kept within a magnetic field of 130 mT for 10 min until completion of fibrin gelation (Supporting Information Figure 11b, c). We found a microgel concentration-dependent effect on cytoskeleton elongation and orientation. A hybrid hydrogel with 0.5 to 1.0 vol % microgels showed fibroblast growth in all three dimensions (Supporting Information Figure 12). However, by applying a concentration of 1.5 vol % microgels or higher, which corresponds to a mean microgel distance of 27.7 μm or less, fibroblasts were able to sense the structural guidance cues and grew one-dimensionally along the microgel orientation (Figure 4a,b; Supporting Information Figure 12). As star-PEG-A does not contain cell adhesion sequences,[36] the cells attached to the fibrin gel, whereas the microgels functioned as physical barriers to induce cell orientation. This reveals that at minimal degrees of material anisotropy, cells decide to grow unidirectionally in 3D, regardless of the fact that the geometrical constrain for orientation, sensed by the cells, is still minimum and would allow nonaligned growth.

To investigate the material's functionality with regard to native oriented tissues, such as nerves, chicken-derived primary dorsal root ganglions (DRGs) were applied. These were inserted into the cast Anisogel solution during the enzymatic cross-linking of the fibrin matrix inside a magnetic field. The constructs were cultured for 5 days and supplemented with nerve growth factor. Initial DRG experiments with 3 vol % microgels, which were either magnetically aligned or left random (Figure 4c), revealed a clear difference with regard to the guidance effect. Here, random microgels led to neurite infiltration without prevalent direction, while aligned microgels induced oriented neurite growth parallel to the noncell adhesive microgels. In this specific example, the presence of buffer around the DRG inhibited fixed microgel alignment adjacent to the DRG, which initially led to random nerve growth but, importantly, once the extending neurites entered the region with the oriented microgels (full white circle) linear neurite

DOI: 10.1021/acs.nanolett.7b01123
Nano Lett. 2017, 17, 3782−3791

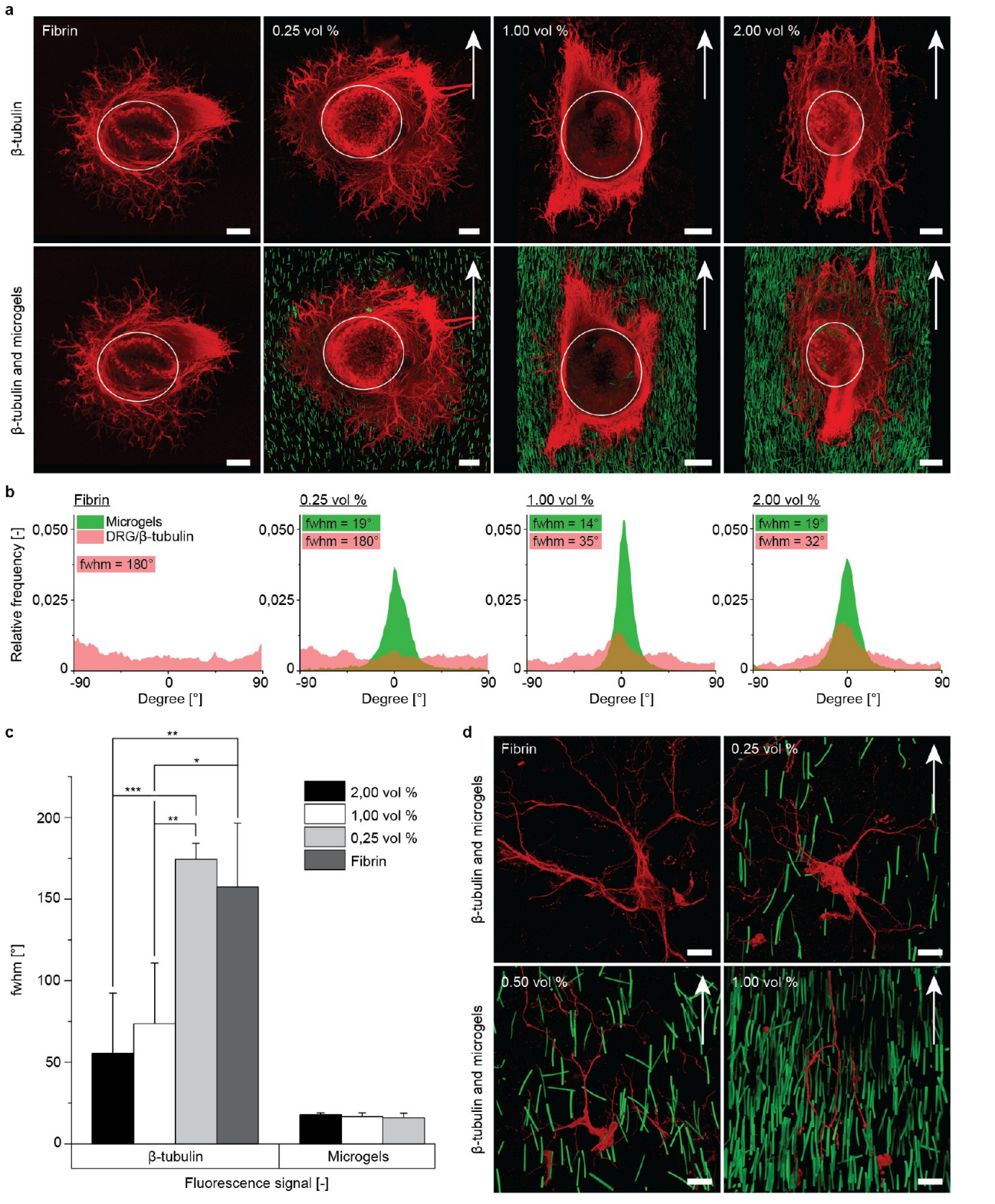

Figure 5. Nerve cells decide to orient in an Anisogel with minimal structural guidance. (a) DRGs (red, Alexa Fluor 633) were inserted in fibrin and Anisogels with 0.25, 1, and 2 vol % microgels (green, fluorescein), revealing that at least 1 vol % is required for nerve guidance. (b) Quantification of the images in (a) substantiates the qualitative findings that 1 vol % microgels is required with no significant improvement for 2 vol %. (c) Full width at half-maximum (fwhm) of quantified neurite extension within the Anisogel (0.25, 1, and 2 vol % microgels) or fibrin. Images were quantified by the imageJ plugin OrientationJ, starting at the edge of the DRG body (marked by white circle) ($n = 3$). (d) Extension of single primary nerve cells mixed within fibrin and Anisogels with 0.25 vol %, 0.5 vol %, and 1 vol %, supporting the threshold of 1 vol % to obtain a functional Anisogel. Data presented as average ± s.d. and statistical significance performed using two-way ANOVA with Bonferroni comparison (*$p < 0.05$; **$p < 0.01$; ***$p < 0.001$). Scale bars in (a) are 200 μm and in (d) 50 μm.

DOI: 10.1021/acs.nanolett.7b01123
Nano Lett. 2017, 17, 3782−3791

infiltration was induced along their orientation. In addition, neurite extension perpendicular to the microgel orientation was blocked. Structure analysis of the images quantified the orientation of the infiltrating neurites in the matrices and confirmed the induced directionality of extending axons (Figure 4d). The full widths at half-maximum (fwhm) of the neurite and microgel orientation distribution were 38° and 19°, respectively, in comparison to 180° for both in the case of nonoriented microgels.

To determine which degree of structure in three dimensions is required to align infiltrating neurites, DRGs were cultivated within Anisogels with different microgel contents (Figure 5a). Contrary to the reported results with fibroblasts (Supporting Information Figure 12b), 1.0 vol % aligned microgels (mean intermicrogel distance of 33.6 μm) in fibrin was sufficient to orient neurite outgrowth. An increase in microgel content to 2.0 vol % did not significantly enhance nerve guidance, while a decrease to 0.25 vol % was insufficient to align the neurites. These findings are supported by the quantification of the DRG alignment via OrientationJ (Figure 5b), showing fwhm's for aligned nerve growth of 73.7° ± 37.1° for 1 vol % and 55.7 ± 36.7° for 2 vol %, which are both significantly lower than the fwhm's calculated for 0.25 vol % and fibrin without microgels (Figure 5c). Even though a small reduction in the fwhm was observed from 1 to 2 vol %, this difference was not statistically significant. Although up to 99% of the volume is available for the infiltrating neurites to grow randomly, the minimal structure is sufficient to trigger the nerves' decision toward oriented neurite extension.

In order to investigate the effect of structural guidance on single neurons, DRGs were dissociated and primary chicken-derived neurons were isolated. The single neurons were cultured in a fibrin gel or Anisogels with 0.25, 0.5, and 1 vol %, confirming that 1 vol % microgels were sufficient to achieve a strong guidance effect (Figure 5d, Movie S3). In the case of 0.5 vol % microgels, neurons could still grow in an aligned manner but would sometime alter their direction to then continue growing parallel to the oriented direction again. These results validated that a minimal amount of structural guidance can trigger nerves to grow in a linear manner, demonstrating the applicability of an Anisogel for the regeneration of sensitive and oriented tissues.

Conclusion. In summary, we present a novel hierarchically designed material class with the ability to direct cell and nerve growth and the potential to regenerate sensitive tissues, which require injectable anisotropic structures. Magnetoceptive, anisometric microgels were applied as building blocks to create a unidirectional structure. The developed technology provides high control over numerous parameters, such as microgel dimensions, shape, stiffness, porosity, water and SPION content. This enables tailoring of the microgel properties and thus the macro- and microenvironment according to the cell's and tissue's demands. We demonstrate that depending on the sensitivity of the cell type, a minimal microgel concentration is required to trigger cell alignment in 3D. Interestingly, both fibroblasts and nerve cells were able to decide to grow unidirectionally inside the anisotropic injectable hydrogels at relatively large distances between the structural guidance cues. The developed Anisogel represents a novel and versatile tissue regenerative material, which fills a gap between the existing implantable constructs and injectable materials. It is the first biomaterial that can achieve highly controlled and ordered structures in situ after injection to guide cell and nerve growth. This feature has the potential to enhance tissue functionality that depends on its structural organization and could be groundbreaking as supporting therapeutic material for spinal cord repair.

■ ASSOCIATED CONTENT

Supporting Information

The Supporting Information is available free of charge on the ACS Publications website at DOI: 10.1021/acs.nanolett.7b01123.

List of materials and methods; Supplementary references; Supplementary figures including: (1) influence of solvent in PRINT process, (2) hydrogel disk fabrication and PEG-based solvent extraction, (3) images of star-PEG hydrogels with different compositions, (4) images of star-PEG hydrogel swelling, (5) cryo-FESEM images of different star-PEG hydrogel compositions with short sublimation time, (6) cryo-FESEM images of different star-PEG hydrogel compositions with long sublimation time, (7) FESEM images of cryo-cuts of different star-PEG hydrogel compositions, (8) cryo-FESEM images of different 20 wt/vol % star-PEG microgel compositions, (9) TEM of SPION-containing microgel, (10) graphical explanation of magnetic alignment time determination methodology, (11, 12) supporting cell culture experiments. Supplementary Table 1: List of interfacial tensions of star-PEG prepolymer compositions. (PDF)
Orientation of microgels (AVI)
Interaction of microgels in high magnetic field (AVI)
Three-dimensional confocal image of single nerves in Anisogel with 1 vol % microgels (AVI)

■ AUTHOR INFORMATION

Corresponding Author

*E-mail: delaporte@dwi.rwth-aachen.de.

ORCID

Martin Möller: 0000-0002-5955-4185

Author Contributions

J.C.R. performed the microgel fabrication, hydrogel characterization, analysis of magnetoceptive microgels, and cell culture experiments and wrote the manuscript. J.K. synthesized star-PEG-A, M.C.T. performed hydrogel characterization experiments, and K.R. contributed to electron microscopy analysis. M.M. provided intellectual contribution to the project. L.D.L. designed the concept, supervised the project, and wrote the manuscript.

Funding

European Research Council (ERC) under the European Union's Horizon 2020 research and innovation program (ANISOGEL, Grant Agreement 637853); Deutsche Forschungsgemeinschaft (DFG) within the SFB 985 "Functional Microgels and Microgel Systems"; EU and the federal state of North Rhine-Westphalia (Grant EFRE 30 00 883 02).

Notes

The authors declare no competing financial interest.

■ ACKNOWLEDGMENTS

We thank Dr. H. Thomas, S. Moli, N. Jansen, S. Mallmann, C. Pörschke, and R. Jansen for experimental assistance. We acknowledge funding from the European Research Council (ERC) under the European Union's Horizon 2020 research

DOI: 10.1021/acs.nanolett.7b01123
Nano Lett. 2017, 17, 3782−3791

and innovation programme (ANISOGEL, Grant Agreement 637853), and the Deutsche Forschungsgemeinschaft (DFG) within the SFB 985 "Functional Microgels and Microgel Systems". This work was performed in part at the Center for Chemical Polymer Technology CPT, which was supported by the EU and the federal state of North Rhine-Westphalia (Grant EFRE 30 00 883 02).

■ ABBREVIATIONS

Anisogel	anisotropic, injectable hybrid hydrogel
DMSO	dimethyl sulfoxide
DRG	dorsal root ganglion
ECM	Extracellular matrix
FESEM	field emission scanning electron microscopy
fwhm	full width at half-maximum
MW	molecular weight
PBS	phosphate buffered saline
PEG-OH	poly(ethylene glycol)
PFPE	perfluoropolyether
RIPD	reaction-induced phase decomposition
SPION	superparamagnetic iron oxide nanoparticle
Star-PEG-A	star-shaped poly(ethylene oxide-*stat*-propylene oxide)-acrylate
Star-PEG-OH	star-shaped poly(ethylene oxide-*stat*-propylene oxide)
TEM	transmission electron microscopy
UHMR	ultrahigh magnetic response

■ REFERENCES

(1) (a) Trappmann, B.; Gautrot, J. E.; Connelly, J. T.; Strange, D. G. T.; Li, Y.; Oyen, M. L.; Stuart, M. A. C.; Boehm, H.; Li, B. J.; Vogel, V.; Spatz, J. P.; Watt, F. M.; Huck, W. T. S. Extracellular-matrix tethering regulates stem-cell fate. *Nat. Mater.* **2012**, *11* (7), 642−649. (b) Geiger, B.; Spatz, J. P.; Bershadsky, A. D. Environmental sensing through focal adhesions. *Nat. Rev. Mol. Cell Biol.* **2009**, *10* (1), 21−33.

(2) (a) Lutolf, M. P.; Hubbell, J. A. Synthetic biomaterials as instructive extracellular microenvironments for morphogenesis in tissue engineering. *Nat. Biotechnol.* **2005**, *23* (1), 47−55. (b) Place, E. S.; Evans, N. D.; Stevens, M. M. Complexity in biomaterials for tissue engineering. *Nat. Mater.* **2009**, *8* (6), 457−470. (c) Young, J. L.; Holle, A. W.; Spatz, J. P. Nanoscale and mechanical properties of the physiological cell-ECM microenvironment. *Exp. Cell Res.* **2016**, *343* (1), 3−6. (d) Rice, J. J.; Martino, M. M.; De Laporte, L.; Tortelli, F.; Briquez, P. S.; Hubbell, J. A. Engineering the Regenerative Microenvironment with Biomaterials. *Adv. Healthcare Mater.* **2013**, *2* (1), 57−71.

(3) Gauvin, R.; Khademhosseini, A. Microscale Technologies and Modular Approaches for Tissue Engineering: Moving toward the Fabrication of Complex Functional Structures. *ACS Nano* **2011**, *5* (6), 4258−4264.

(4) (a) De Laporte, L.; Yang, Y.; Zelivyanskaya, M. L.; Cummings, B. J.; Anderson, A. J.; Shea, L. D. Plasmid releasing multiple channel bridges for transgene expression after spinal cord injury. *Mol. Ther.* **2009**, *17* (2), 318−326. (b) Yang, Y.; De Laporte, L.; Zelivyanskaya, M. L.; Whittlesey, K. J.; Anderson, A. J.; Cummings, B. J.; Shea, L. D. Multiple channel bridges for spinal cord injury: cellular characterization of host response. *Tissue Eng., Part A* **2009**, *15* (11), 3283−3295. (c) Gao, M.; Lu, P.; Bednark, B.; Lynam, D.; Conner, J. M.; Sakamoto, J.; Tuszynski, M. H. Templated agarose scaffolds for the support of motor axon regeneration into sites of complete spinal cord transection. *Biomaterials* **2013**, *34* (5), 1529−1536.

(5) (a) Xie, J. W.; Liu, W. Y.; MacEwan, M. R.; Bridgman, P. C.; Xia, Y. N. Neurite Outgrowth on Electrospun Nanofibers with Uniaxial Alignment: The Effects of Fiber Density, Surface Coating, and Supporting Substrate. *ACS Nano* **2014**, *8* (2), 1878−1885. (b) Schnell, E.; Klinkhammer, K.; Balzer, S.; Brook, G.; Klee, D.; Dalton, P.; Mey, J. Guidance of glial cell migration and axonal growth on electrospun nanofibers of poly-ε-caprolactone and a collagen/poly-ε-caprolactone blend. *Biomaterials* **2007**, *28* (19), 3012−3025. (c) Kriebel, A.; Rumman, M.; Scheld, M.; Hodde, D.; Brook, G.; Mey, J. Three-dimensional configuration of orientated fibers as guidance structures for cell migration and axonal growth. *J. Biomed. Mater. Res., Part B* **2014**, *102* (2), 356−365.

(6) Macaya, D.; Spector, M. Injectable hydrogel materials for spinal cord regeneration: a review. *Biomed. Mater.* **2012**, *7* (1), 012001.

(7) Li, X.; Zhou, J.; Liu, Z. Q.; Chen, J.; Lu, S. H.; Sun, H. Y.; Li, J. J.; Lin, Q. X.; Yang, B. G.; Duan, C. M.; Xing, M.; Wang, C. Y. A PNIPAAm-based thermosensitive hydrogel containing SWCNTs for stem cell transplantation in myocardial repair. *Biomaterials* **2014**, *35* (22), 5679−5688.

(8) Cheng, T. Y.; Chen, M. H.; Chang, W. H.; Huang, M. Y.; Wang, T. W. Neural stem cells encapsulated in a functionalized self-assembling peptide hydrogel for brain tissue engineering. *Biomaterials* **2013**, *34* (8), 2005−2016.

(9) Yu, L.; Ding, J. D. Injectable hydrogels as unique biomedical materials. *Chem. Soc. Rev.* **2008**, *37* (8), 1473−1481.

(10) Li, Y. F.; Fang, X. Q.; Jiang, T. Minimally traumatic alveolar ridge augmentation with a tunnel injectable thermo-sensitive alginate scaffold. *J. Appl. Oral Sci.* **2015**, *23* (2), 215−223.

(11) Tan, H. P.; Chu, C. R.; Payne, K. A.; Marra, K. G. Injectable in situ forming biodegradable chitosan-hyaluronic acid based hydrogels for cartilage tissue engineering. *Biomaterials* **2009**, *30* (13), 2499−2506.

(12) Griffin, D. R.; Weaver, W. M.; Scumpia, P. O.; Di Carlo, D.; Segura, T. Accelerated wound healing by injectable microporous gel scaffolds assembled from annealed building blocks. *Nat. Mater.* **2015**, *14* (7), 737−44.

(13) Seliktar, D. Designing Cell-Compatible Hydrogels for Biomedical Applications. *Science* **2012**, *336* (6085), 1124−1128.

(14) Dubey, N.; Letourneau, P. C.; Tranquillo, R. T. Neuronal contact guidance in magnetically aligned fibrin gels: effect of variation in gel mechano-structural properties. *Biomaterials* **2001**, *22* (10), 1065−1075.

(15) Ceballos, D.; Navarro, X.; Dubey, N.; Wendelschafer-Crabb, G.; Kennedy, W. R.; Tranquillo, R. T. Magnetically aligned collagen gel filling a collagen nerve guide improves peripheral nerve regeneration. *Exp. Neurol.* **1999**, *158* (2), 290−300.

(16) Zhang, S.; Greenfield, M. A.; Mata, A.; Palmer, L. C.; Bitton, R.; Mantei, J. R.; Aparicio, C.; de la Cruz, M. O.; Stupp, S. I. A self-assembly pathway to aligned monodomain gels. *Nat. Mater.* **2010**, *9* (7), 594−601.

(17) Berns, E. J.; Sur, S.; Pan, L.; Goldberger, J. E.; Suresh, S.; Zhang, S.; Kessler, J. A.; Stupp, S. I. Aligned neurite outgrowth and directed cell migration in self-assembled monodomain gels. *Biomaterials* **2014**, *35* (1), 185−195.

(18) Kim, J.; Staunton, J. R.; Tanner, K. Independent Control of Topography for 3D Patterning of the ECM Microenvironment. *Adv. Mater.* **2016**, *28* (1), 132−137.

(19) Antman-Passig, M.; Shefi, O. Remote Magnetic Orientation of 3D Collagen Hydrogels for Directed Neuronal Regeneration. *Nano Lett.* **2016**, *16*, 2567.

(20) Pisanic, T. R., 2nd; Blackwell, J. D.; Shubayev, V. I.; Finones, R. R.; Jin, S. Nanotoxicity of iron oxide nanoparticle internalization in growing neurons. *Biomaterials* **2007**, *28* (16), 2572−81.

(21) Erb, R. M.; Libanori, R.; Rothfuchs, N.; Studart, A. R. Composites reinforced in three dimensions by using low magnetic fields. *Science* **2012**, *335* (6065), 199−204.

(22) Rolland, J. P.; Maynor, B. W.; Euliss, L. E.; Exner, A. E.; Denison, G. M.; DeSimone, J. M. Direct fabrication and harvesting of monodisperse, shape-specific nanobiomaterials. *J. Am. Chem. Soc.* **2005**, *127* (28), 10096−10100.

(23) Neuerburg, C.; Recknagel, S.; Fiedler, J.; Groll, J.; Moeller, M.; Bruellhoff, K.; Reichel, H.; Ignatius, A.; Brenner, R. E. Ultrathin sP(EO-stat-PO) hydrogel coatings are biocompatible and preserve

DOI: 10.1021/acs.nanolett.7b01123
Nano Lett. 2017, 17, 3782−3791

functionality of surface bound growth factors in vivo. *J. Mater. Sci.: Mater. Med.* **2013**, *24* (10), 2417−27.
(24) Williams, S. S.; Retterer, S.; Lopez, R.; Ruiz, R.; Samulski, E. T.; DeSimone, J. M. High-Resolution PFPE-based Molding Techniques for Nanofabrication of High-Pattern Density, Sub-20 nm Features: A Fundamental Materials Approach. *Nano Lett.* **2010**, *10* (4), 1421−1428.
(25) (a) Xu, S.; Nie, Z.; Seo, M.; Lewis, P.; Kumacheva, E.; Stone, H. A.; Garstecki, P.; Weibel, D. B.; Gitlin, I.; Whitesides, G. M. Generation of monodisperse particles by using microfluidics: control over size, shape, and composition. *Angew. Chem., Int. Ed.* **2005**, *44* (5), 724−8. (b) Bhaskar, S.; Hitt, J.; Chang, S.-W. L.; Lahann, J. Multicompartmental Microcylinders. *Angew. Chem., Int. Ed.* **2009**, *48* (25), 4589−4593.
(26) Merkel, T. J.; Chen, K.; Jones, S. W.; Pandya, A. A.; Tian, S. M.; Napier, M. E.; Zamboni, W. E.; DeSimone, J. M. The effect of particle size on the biodistribution of low-modulus hydrogel PRINT particles. *J. Controlled Release* **2012**, *162* (1), 37−44.
(27) (a) Skardal, A.; Devarasetty, M.; Kang, H.-W.; Mead, I.; Bishop, C.; Shupe, T.; Lee, S. J.; Jackson, J.; Yoo, J.; Soker, S.; Atala, A. A hydrogel bioink toolkit for mimicking native tissue biochemical and mechanical properties in bioprinted tissue constructs. *Acta Biomater.* **2015**, *25*, 24−34. (b) Browning, M. B.; Cereceres, S. N.; Luong, P. T.; Cosgriff-Hernandez, E. M. Determination of the in vivo degradation mechanism of PEGDA hydrogels. *J. Biomed. Mater. Res., Part A* **2014**, *102* (12), 4244−4251. (c) van den Brand, R.; Heutschi, J.; Barraud, Q.; DiGiovanna, J.; Bartholdi, K.; Huerlimann, M.; Friedli, L.; Vollenweider, I.; Moraud, E. M.; Duis, S.; Dominici, N.; Micera, S.; Musienko, P.; Courtine, G. Restoring Voluntary Control of Locomotion after Paralyzing Spinal Cord Injury. *Science* **2012**, *336* (6085), 1182−1185. (d) Discher, D. E.; Janmey, P.; Wang, Y. L. Tissue cells feel and respond to the stiffness of their substrate. *Science* **2005**, *310* (5751), 1139−1143.
(28) Inoue, T. Reaction-induced phase decomposition in polymer blends. *Prog. Polym. Sci.* **1995**, *20* (1), 119−153.
(29) Caliari, S. R.; Burdick, J. A. A practical guide to hydrogels for cell culture. *Nat. Methods* **2016**, *13* (5), 405−414.
(30) Hollister, S. J. Porous scaffold design for tissue engineering. *Nat. Mater.* **2005**, *4* (7), 518−524.
(31) Galaev, I. M. B. *Smart Polymers Applications in Biotechnology and Biomedicine*, 2nd ed.; CPC Press: Boca Raton, 2008.
(32) Kanamori, K.; Hasegawa, J.; Nakanishi, K.; Hanada, T. Facile Synthesis of Macroporous Cross-Linked Methacrylate Gels by Atom Transfer Radical Polymerization. *Macromolecules* **2008**, *41* (19), 7186−7193.
(33) (a) Luo, W.; Nagel, S. R.; Rosenbaum, T. F.; Rosensweig, R. E. Dipole interactions with random anisotropy in a frozen ferrofluid. *Phys. Rev. Lett.* **1991**, *67* (19), 2721−2724. (b) Leshansky, A. M.; Morozov, K. I.; Rubinstein, B. Y. Shape-controlled anisotropy of superparamagnetic micro-/nanohelices. *Nanoscale* **2016**, *8*, 14127.
(34) Nunes, J.; Herlihy, K. P.; Mair, L.; Superfine, R.; DeSimone, J. M. Multifunctional Shape and Size Specific Magneto-Polymer Composite Particles. *Nano Lett.* **2010**, *10* (4), 1113−1119.
(35) Ryan, E. A.; Mockros, L. F.; Weisel, J. W.; Lorand, L. Structural origins of fibrin clot rheology. *Biophys. J.* **1999**, *77* (5), 2813−26.
(36) (a) Grafahrend, D.; Heffels, K.-H.; Beer, M. V.; Gasteier, P.; Möller, M.; Boehm, G.; Dalton, P. D.; Groll, J. Degradable polyester scaffolds with controlled surface chemistry combining minimal protein adsorption with specific bioactivation. *Nat. Mater.* **2011**, *10* (1), 67−73. (b) Perry, J. L.; Reuter, K. G.; Kai, M. P.; Herlihy, K. P.; Jones, S. W.; Luft, J. C.; Napier, M.; Bear, J. E.; DeSimone, J. M. PEGylated PRINT Nanoparticles: The Impact of PEG Density on Protein Binding, Macrophage Association, Biodistribution, and Pharmacokinetics. *Nano Lett.* **2012**, *12* (10), 5304−5310.

DOI: 10.1021/acs.nanolett.7b01123
Nano Lett. 2017, 17, 3782−3791